ChemComm

COMMUNICATION

View Article Online
View Journal | View Issue

Cite this: *Chem. Commun.*, 2024, **60**, 13059

Received 21st August 2024,
Accepted 14th October 2024

DOI: 10.1039/d4cc04269g

rsc.li/chemcomm

Aliovalent metal cation doping of $La_5Ti_2AgO_7S_5$ particles for improved photocatalytic and photoelectrochemical water splitting†

Yosuke Kageshima, *[ab] Shiino Otsuka,[a] Ryunosuke Iwaya,[a] Haruto Yonehara,[a] Katsuya Teshima, [ab] Kazunari Domen [bc] and Hiromasa Nishikiori *[ab]

The doping of photocatalytic $La_5Ti_2AgO_7S_5$ particles with aliovalent metal cations was investigated. The incorporation of lower-valence Al^{3+} cations at Ti^{4+} sites improved the photocatalytic hydrogen evolution activity. In addition, the anodic photocurrent during oxygen evolution was increased upon adding higher-valence Ta^{5+} ions. The effect of doping on the carrier density in the photocatalytic particles was also examined in this work.

Photocatalytic and photoelectrochemical (PEC) water splitting are regarded as key technologies associated with the future development of artificial photosynthetic systems.[1] Because a large portion of solar radiation consists of visible light, the design of visible-light-responsive photocatalytic materials is an important aspect of such systems.[2] Particulate $La_5Ti_2AgO_7S_5$ (LTA) is one of the most promising candidates for this purpose, as this material can absorb visible light up to approximately 570 nm.[3] Compared with conventional sulphides such as CdS, oxysulphide particles are also relatively resistant to photocorrosion and are thus capable of driving the photocatalytic hydrogen or oxygen evolution half-reactions in a reasonably stable manner.[3a] Electrodes fabricated from LTA powder have also been reported to generate both cathodic and anodic photocurrents in response to visible light.[3b] Thus, LTA particles could function as hydrogen or oxygen-evolving components of overall water splitting systems based on two-step photoexcitation processes, such as PEC cells or Z-scheme powder suspension systems.

Various approaches to the design of efficient photocatalytic particles have been proposed. As an example, there have been several reports of improvements in the photocatalytic and PEC performance of $La_5Ti_2CuO_7S_5$, which possesses the same crystalline structure as LTA, following doping with metal cations or surface modifications.[4] Even so, such techniques have rarely been applied to LTA and so the photocatalytic and PEC activities of this material could potentially be enhanced.

The present work investigated the incorporation of aliovalent metal cations (*i.e.*, Al^{3+} or Ta^{5+}) at Ti^{4+} sites in LTA to increase the photocatalytic and PEC water splitting performance of this material. Photocatalytic hydrogen or oxygen evolution half-reactions as well as PEC oxygen evolution trials were subsequently performed using doped LTA specimens. The origin of any changes in activity after doping were elucidated by examining the effect on carrier density in the particulate LTA. The experimental details and results from optimisation of the cocatalyst modification procedures (Fig. S1) are provided in the ESI.†[3–5]

Scanning electron microscopy (SEM) images showed that the synthesised LTA comprised rod-like crystals approximately 1 μm in diameter and with lengths on the order of 10 μm (Fig. 1a).[3] Doping with Al^{3+} or Ta^{5+} had a minimal effect on the morphology of these particles regardless of the doping level (Fig. S2, ESI†). Diffuse reflectance (DR) spectra were acquired from the LTA, Al-doped LTA (Al:LTA) and Ta-doped LTA (Ta:LTA) specimens and are presented in Fig. 1b. The Al:LTA samples were found to have absorption edges almost identical to that for LTA at approximately 570 nm, regardless of the degree of doping (Fig. S3, ESI†). In contrast, the absorption edges for the Ta:LTA specimens were slightly red-shifted with increasing extent of doping (Fig. S3, ESI†). Increasing the amount of Ta in the material also led to higher absorbance at wavelengths longer than the absorption edge. This increased baseline absorption can possibly be attributed to the presence of defect sites.[6] X-ray diffraction (XRD) patterns for the materials suggested that highly pure LTA was obtained regardless of the presence or absence of dopants (Fig. 1c and Fig. S4, ESI†). The positions of diffraction peaks related to (714) planes as functions of the doping level are plotted in Fig. 1d. In the case

[a] *Department of Materials Chemistry, Faculty of Engineering, Shinshu University, 4-17-1 Wakasato, Nagano 380–8553, Japan. E-mail: kage_ysk@shinshu-u.ac.jp, nishiki@shinshu-u.ac.jp*
[b] *Research Initiative for Supra-Materials (RISM), Shinshu University, 4–17-1 Wakasato, Nagano 380–8553, Japan*
[c] *Office of University Professors, The University of Tokyo, 7-3-1 Hongo, Bunkyo-ku, Tokyo 113-8656, Japan*

† Electronic supplementary information (ESI) available: Experimental details and supporting figures. See DOI: https://doi.org/10.1039/d4cc04269g

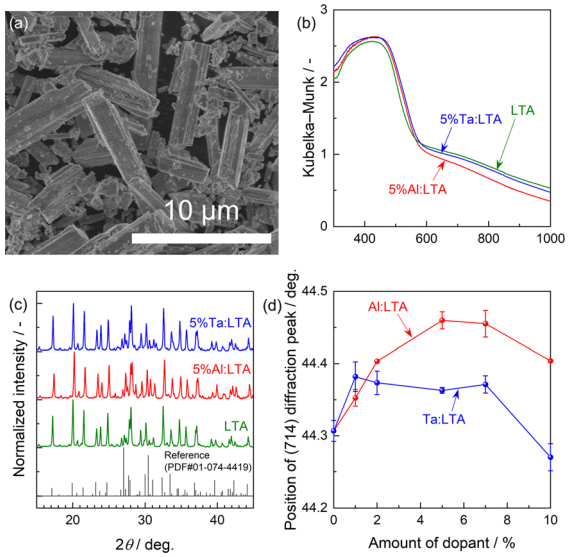

Fig. 1 (a) An SEM image of the LTA. (b) DR spectra and (c) XRD patterns of the LTA and doped LTA specimens. (d) Positions of (714) diffraction peaks as functions of the doping level.

of the Al:LTA, there was a slight shift to higher angle with greater amount of doping whereas the addition of Ta^{5+} had little effect. The ionic radii of La^{3+}, Ti^{4+}, Ag^{+}, Al^{3+} and Ta^{5+} in a four-coordinated state are 103, 61, 115, 54 and 64 pm, respectively. If Al^{3+} and Ta^{5+} are substituted into La^{3+} or Ag^{+} sites, significant diffraction peak shifts would therefore be expected due to the large differences in ionic radii. The trends exhibited by the XRD peak shifts in Fig. 1d can be attributed to decreases in the lattice constant caused by doping with Al^{3+}, which is slightly smaller than Ti^{4+}, and a limited effect of doping with Ta^{5+}, which has an almost identical ionic radius to that of Ti^{4+}. On this basis, it appears that the Al^{3+} and Ta^{5+} ions were likely incorporated into the LTA at Ti^{4+} sites. It should be noted that the diffraction peak shifts observed in the case of the Al:LTA essentially plateaued at doping levels above 10 mol%, indicating that the solid solubility limit of the present dopants might be less than approximately 10 mol%. Distribution and homogeneity of the dopant species in the photocatalyst crystals were discussed in the ESI† (Fig. S5–S7). The excess dopants that were not doped into the lattice may exist separately from the LTA particles rather than fragment-like nanoparticles deposited on the photocatalyst surface. Nevertheless, the above characterisations demonstrate that the synthesised specimens exhibited morphologies, optical properties and crystalline structures consistent with those reported for LTA,[3] confirming the successful synthesis of doped LTA samples.

The doped materials were found to promote steady hydrogen or oxygen evolution half-reactions under visible light (Fig. S8, ESI†). The initial hydrogen evolution rates are plotted as functions of the doping level in Fig. 2a. Increasing the Al^{3+} doping level gradually improved the hydrogen evolution activity, with 5 mol% Al^{3+} giving the highest activity. In contrast, the incorporation of Ta^{5+} doping seriously deteriorated the hydrogen evolution activity. The present aliovalent doping did not

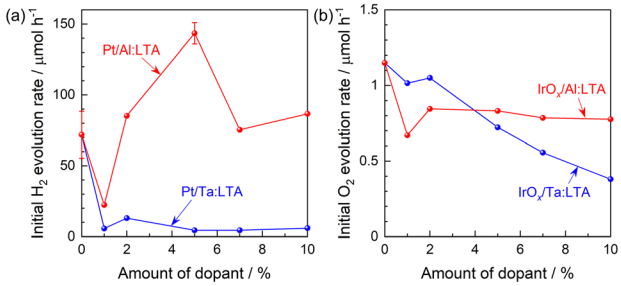

Fig. 2 Initial photocatalysis rates as functions of doping level as determined for the (a) hydrogen evolution and (b) oxygen evolution half-reactions under illumination with a 300 W Xe lamp (λ = 420–800 nm).

improve the oxygen evolution activity regardless of the type or amount of dopant, as shown in Fig. 2b. The oxygen evolution activity was also found to be essentially unaffected by the Al^{3+} doping level but gradually decreased with increasing amount of Ta^{5+}. Only doping with the lower-valence Al^{3+} cations at Ti^{4+} sites improved the photocatalytic hydrogen evolution activity.

Typical current–potential curves for the cobalt-phosphate (CoPi)-modified LTA, Al:LTA and Ta:LTA particulate photoelectrodes in a Na_2SO_4 electrolyte under simulated sunlight are provided in Fig. 3a. Separate optimisation trials suggested that a 5 mol% doping level was suitable for PEC application (Fig. S9, ESI†). Anodic photocurrents were generated by the LTA, Al:LTA and Ta:LTA at potentials more positive than 0, 0.2 and 0.1 V *vs.* a reversible hydrogen electrode (RHE), respectively, and these currents gradually increased as more positive potentials were applied (Fig. 3a). The present specimens exhibited significantly negative onset potentials for anodic photocurrents, in the vicinity of 0 V_{RHE}, under simulated sunlight. Here, it should be considered that the onset potentials of most visible-light-responsive photoanodes are usually observed at approximately 0.6 V_{RHE},[7] and that the Cu-containing counterpart materials (such as $La_5Ti_2Cu_{1-x}Ag_xO_7S_5$) could serve only as hydrogen-evolving photocathodes.[4c] Hence, it appears that LTA could serve as an oxygen-evolving photoanode material in PEC overall water splitting systems based on a two-step photoexcitation process. The Ta:LTA produced higher anodic photocurrents than the pristine LTA at positive potentials while Al^{3+} doping significantly decreased the photocurrent at negative applied

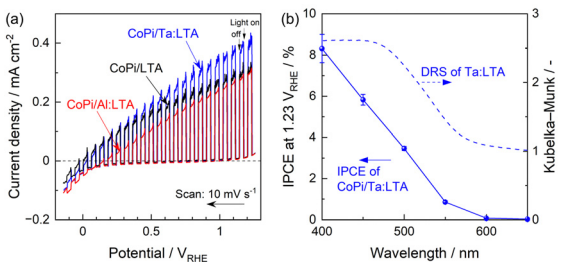

Fig. 3 (a) Current–potential curves obtained using CoPi-modified LTA, 5%Al-doped LTA and 5%Ta-doped LTA in aqueous 0.5 M Na_2SO_4 solutions under simulated sunlight. (b) The IPCE spectrum for the CoPi/Ta:LTA photoanode at an applied potential of 1.23 V_{RHE} together with the DR spectrum of the Ta:LTA particles.

potentials. Additionally, the Al:LTA showed a cathodic photoresponse at negative potentials in the vicinity of 0 V_{RHE}, implying enhanced p-type semiconductor characteristics. These observations indicate that n-type doping (that is, doping of Ta^{5+} at Ti^{4+} sites) likely improved the PEC performance due to increase in conductivity.[8] The half-cell solar-to-hydrogen (HC-STH) energy conversion efficiencies are presented in Fig. S10 (ESI†). The maximum HC-STH values obtainable from the LTA, Al:LTA and Ta:LTA were 0.11% (at 0.55 V_{RHE}), 0.088% (at 0.68 V_{RHE}) and 0.14% (at 0.56 V_{RHE}), respectively. The Ta:LTA provided higher HC-STH values compared with the undoped LTA at potentials more positive than 0.2 V_{RHE} whereas the values for the Al-doped specimens were less than those for the undoped materials. The incident-photon-to-current conversion efficiency (IPCE) spectrum of the CoPi/Ta:LTA photoanode is shown in Fig. 3b together with the DR spectrum of the material. The onset of the IPCE spectrum is in good agreement with the absorption edge for the specimen, confirming that the photocurrent originated solely from bandgap photoexcitation of the Ta:LTA. Monochromatic light at wavelengths longer than 600 nm did not produce a photocurrent, indicating that baseline absorption by this material did not contribute to the PEC reaction.[6] It was confirmed that the simple mixing Al_2O_3 or Ta_2O_5 impurities with LTA barely enhanced the photocatalytic or PEC activity (Fig. S11, ESI†).

The effect of aliovalent doping on the carrier density in the LTA particles was examined based on electrochemical impedance measurements. It should be noted that, in the case of particulate photoelectrodes prepared by the particle transfer (PT) method, the backside metal electrode is partially in contact with the electrolyte through the interstitial spaces between neighbouring semiconductor particles. If an undesirable interface between the metal and electrolyte coexists in parallel with the semiconductor/electrolyte interface, there will be a risk of incorrect evaluation of the latter circuit. To address this issue, the semiconductor particles/metal foil assembly fabricated through the PT method was fixed on a secondary glass substrate using an epoxy resin, as an alternative to the double-sided carbon tape that had been typically used for this fixation process. The epoxy resin penetrated through voids in the backside metal foil and so sealed the spaces between the semiconductor particles.[9] This enabled the impedance analyses to assess solely the semiconductor/electrolyte interface. Details of this process are provided in Fig. S12 (ESI†). The Mott–Schottky plots obtained from undoped LTA, Al:LTA and Ta:LTA particulate photoanodes without cocatalysts are presented in Fig. 4a. Each of the specimens generated a positive slope, indicating that n-type semiconductivity was obtained regardless of the type of dopant. The Al:LTA produced a larger slope than the undoped specimen whereas the Ta:LTA generated a smaller slope. Because the present doping process was found to have essentially no effect on the morphology and size of the LTA particles, the surface area of the semiconductor/electrolyte interface would also be expected to be independent of the type of dopant. Therefore, it can be concluded that Al or Ta doping decreased or increased the carrier density in the LTA particles, respectively.

In prior studies of particulate photocatalyst dispersion systems, doping with lower-valence cations has been demonstrated to enhance the photocatalytic activity.[10] When the carrier density in an n-type semiconductor decreases (that is, the Fermi level of the semiconductor is shifted in the positive direction), the height of the Schottky-like barrier formed between the semiconductor and electrolyte at equilibrium under dark conditions should decrease (Fig. 4b and c). This effect could promote the reaction of photogenerated electrons with water immediately after the onset of light exposure. Hence, photocatalytic activity associated with the hydrogen evolution half-reaction could be improved. However, decreasing the barrier height can also lower the driving force for photoexcited minority carriers (*i.e.*, holes). The balance between these favourable and adverse effects could be responsible for the lack of any change in oxygen evolution activity with Al^{3+} doping. In the case of Ta^{5+} doping, increasing the barrier height at the solid–liquid interface at equilibrium under dark conditions could prevent electrons from reacting with water (Fig. 4b and d). Photocatalysis requires equal quantities of photogenerated electrons and holes to be consumed at the photocatalyst surface. Therefore, an extreme lowering of the reactivity of conduction band electrons could also reduce the reactivity of holes. This phenomenon could explain why

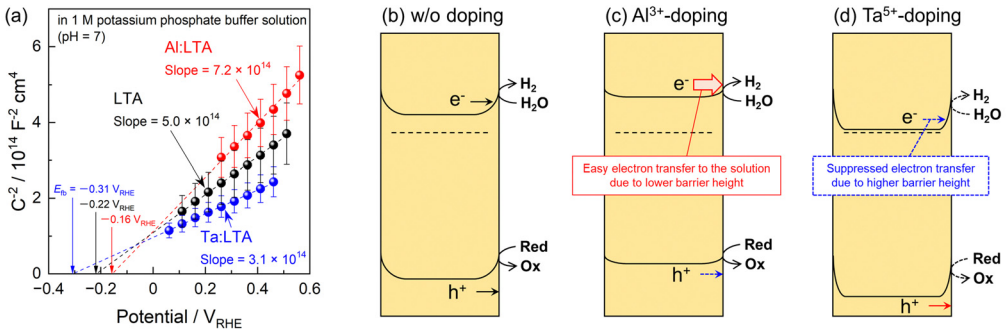

Fig. 4 (a) Mott–Schottky plots obtained from the LTA, 5%Al-doped LTA and 5%Ta-doped LTA photoanodes by applying a potential frequency of 5 kHz in a potassium phosphate buffer electrolyte under dark conditions. Schematic band diagrams for the (b) undoped, (c) Al^{3+}-doped and (d) Ta^{5+}-doped LTA samples at equilibrium in the aqueous solution under dark conditions, demonstrating the effects of aliovalent doping.

Ta^{5+} doping decreased both the hydrogen and oxygen evolution half-reaction activities. Indeed, the incorporation of Al^{3+} or Ta^{5+} positively or negatively shifted the flat-band potential for the material (almost equal to the Fermi level) compared with that for the undoped LTA, respectively (Fig. 4a). In a photoelectrode system, increasing the carrier density by Ta^{5+} doping should improve the bulk conductivity and thus increase the anodic photocurrent. Indeed, doping with higher valence cations has been reported to enhance the PEC performance of many photoanode systems incorporating n-type semiconductors.[8]

Nevertheless, there remains room for improvement in terms of the photocatalytic and PEC performance of doped LTA. The anodic photocurrent values obtained from the present LTA photoanodes were not affected by modification with oxygen-evolving cocatalysts or by adding methanol as a sacrificial hole scavenger to the electrolyte (Fig. S13, ESI†). Photocatalysis and PEC reaction rates are typically governed by both physical processes inside the semiconductor (*e.g.*, photon absorption, charge separation and charge migration) and chemical processes at the catalyst surface.[11] Considering that the photocurrent was not increased even in the case that surface chemical reactions proceeded more easily, it appears that the photocatalytic and PEC performance of the present LTA was primarily determined by the sluggish physical processes inside the semiconductor rather than by water splitting reaction kinetics. Therefore, the performance of LTA could be enhanced in future by improving the bulk properties of the photocatalytic particles. This could be done by optimizing the crystallinity through the exploration of novel synthesis routes[12] or reducing the particle size to decrease the carrier migration length.[13] Additionally, it should be also noted that the present synthesis technique using a sealed vacuum ampule is not suitable for the mass-production and thus it would be necessary to develop flow-type reactor processes in future.[14]

In summary, aliovalent metal cation doping of LTA particles was demonstrated. Doping with Al^{3+}, which has a lower valence state than Ti^{4+}, provided enhanced photocatalytic activity during the hydrogen evolution half-reaction in a powder suspension system. In addition, the incorporation of higher valence Ta^{5+} ions increased the anodic photocurrent provided by photoelectrodes. Impedance analyses suggested that variations in the photocatalytic and PEC performance can be attributed to decreases and increases, respectively, in the carrier density based on adding lower- and higher-valence cations. Aliovalent metal cation doping has represented a common approach to design efficient photocatalytic materials through particle size and morphology control,[15] adjustment of carrier dynamics,[10] and defect engineering.[10] Meanwhile, the present study is expected to provide the comprehensive insight regarding carrier density controlling intended for improved photocatalytic and PEC performance. However, because the performance of the LTA used in this work was primarily limited by the physical processes inside the semiconductor, future work should involve optimizing the bulk properties of the photocatalytic particles.

This work was financially supported by Grants-in-Aid for Scientific Research (B) (no. 21H01715) and for Scientific Research (C) (no. 22K05297) from the Japan Society for the Promotion of Science (JSPS).

Data availability

All relevant data are available from the corresponding authors on request.

Conflicts of interest

There are no conflicts to declare.

Notes and references

1 W. Yang, R. R. Prabhakar, J. Tan, S. D. Tilley and J. Moon, *Chem. Soc. Rev.*, 2019, **48**, 4979.
2 K. Maeda, *J. Photochem. Photobiol., C*, 2011, **12**, 237.
3 (*a*) T. Suzuki, T. Hisatomi, K. Teramura, Y. Shimodaira, H. Kobayashi and K. Domen, *Phys. Chem. Chem. Phys.*, 2012, **14**, 15475; (*b*) M. Katayama, D. Yokoyama, Y. Maeda, Y. Ozaki, M. Tabata, Y. Matsumoto, A. Ishikawa, J. Kubota and K. Domen, *Mater. Sci. Eng. B*, 2010, **173**, 275.
4 (*a*) Z. Song, T. Hisatomi, S. Chen, Q. Wang, G. Ma, S. Li, X. Zhu, S. Sun and K. Domen, *ChemSusChem*, 2019, **12**, 1906; (*b*) J. Liu, T. Hisatomi, D. H. K. Murthy, M. Zhong, M. Nakabayashi, T. Higashi, Y. Suzuki, H. Matsuzaki, K. Seki, A. Furube, N. Shibata, M. Katayama, T. Minegishi and K. Domen, *J. Phys. Chem. Lett.*, 2017, **8**, 375; (*c*) T. Hisatomi, S. Okamura, J. Liu, Y. Shinohara, K. Ueda, T. Higashi, M. Katayama, T. Minegishi and K. Domen, *Energy Environ. Sci.*, 2015, **8**, 3354; (*d*) J. Liu, T. Hisatomi, G. Ma, A. Iwanaga, T. Minegishi, Y. Moriya, M. Katayama, J. Kubota and K. Domen, *Energy Environ. Sci.*, 2014, **7**, 2239.
5 (*a*) F. Takagi, S. Taguchi, Y. Kageshima, K. Teshima, K. Domen and H. Nishikiori, *Appl. Phys. Lett.*, 2021, **119**, 123902; (*b*) Y. Wei, G. Cheng, O. Xiong, F. Xu and R. Chen, *ACS Sustainable Chem. Eng.*, 2017, **5**, 5027; (*c*) T. Minegishi, N. Nishimura, J. Kubota and K. Domen, *Chem. Sci.*, 2013, **4**, 1120.
6 (*a*) K. Maeda, M. Higashi, B. Siritanaratkul, R. Abe and K. Domen, *J. Am. Chem. Soc.*, 2011, **133**, 12334; (*b*) M. Miyauchi, M. Takashio and H. Tobimatsu, *Langmuir*, 2004, **20**, 232.
7 (*a*) G. Liu, S. Ye, P. Yan, F. Xiong, P. Fu, Z. Wang, Z. Chen, J. Shi and C. Li, *Energy Environ. Sci.*, 2016, **9**, 1327; (*b*) J. Seo, T. Takata, M. Nakabayashi, T. Hisatomi, N. Shibata, T. Minegishi and K. Domen, *J. Am. Chem. Soc.*, 2015, **137**, 12780; (*c*) T. W. Kim and K.-S. Choi, *Science*, 2014, **343**, 990; (*d*) M. Higashi, K. Domen and R. Abe, *J. Am. Chem. Soc.*, 2012, **134**, 6968; (*e*) K. Sivula, F. L. Formal and M. Grätzel, *ChemSusChem*, 2011, **4**, 432.
8 (*a*) D. O. B. Apriandanu, S. Nakayama, K. Shibata and F. Amano, *Electrochim. Acta*, 2023, **456**, 142434; (*b*) T. Wang, X. Long, S. Wei, P. Wang, C. Wang, J. Jin and G. Hu, *ACS Appl. Mater. Interfaces*, 2020, **12**, 49705; (*c*) P. Biswas, A. Ainabayev, A. Zhussupbekova, F. Jose, R. O'Connor, A. Kaisha, B. Walls and I. V. Shvets, *Sci. Rep.*, 2020, **10**, 7463; (*d*) L. Pei, B. Lv, S. Wang, Z. Yu, S. Yan, R. Abe and Z. Zou, *ACS Appl. Energy Mater.*, 2018, **1**, 4150; (*e*) F. F. Abdi, N. Firet and R. van de Krol, *ChemCatChem*, 2013, **5**, 490.
9 Y. Kageshima, S. Shiga, H. Kumagai, K. Teshima, K. Domen and H. Nishikiori, *Bull. Chem. Soc. Jpn.*, 2020, **93**, 942.
10 (*a*) L. L. Rusevich, E. A. Kotomin, G. Zvejnieks, M. M. Kržmanc, S. Gupta, N. Daneu, J. C. S. Wu, Y.-G. Lee and W.-Y. Yu, *J. Phys. Chem. C*, 2022, **126**, 21223; (*b*) A. Yamakata, J. J. M. Vequizo, T. Ogawa, K. Kato, S. Tsuboi, N. Furutani, M. Ohtsuka, S. Muto, A. Kuwabara and Y. Sakata, *ACS Catal.*, 2021, **11**, 1911; (*c*) T. Takata and K. Domen, *J. Phys. Chem. C*, 2009, **113**, 19386.
11 K. Takanabe, *ACS Catal.*, 2017, **7**, 8006.
12 M. Cai, X. Wang, J. Xue, Y. Jiang, Y. Wei, Q. Cheng, J. Chen and S. Sun, *Appl. Phys. Lett.*, 2021, **119**, 071903.
13 Z. Pan, Q. Xiao, S. Chen, Z. Wang, L. Lin, M. Nakabayashi, N. Shibata, T. Takata, T. Hisatomi and K. Domen, *J. Catal.*, 2021, **399**, 230.
14 Y. Kageshima, Y. Ooka, H. Kumagai, F. Takagi, K. Teshima, K. Domen and H. Nishikiori, *Sustainable Energy Fuels*, 2023, **7**, 5342.
15 A. Iwase, H. Kato and A. Kudo, *ChemSusChem*, 2009, **2**, 873.

